Postprint of: Ogurtsov S., Kozieł S., A Conformal Circularly Polarized Series-Fed Microstrip Antenna Array Design, IEEE TRANSACTIONS ON ANTENNAS AND PROPAGATION, Vol. 68, iss. 2 (2020), pp. 873-881, DOI: 10.1109/TAP.2019.2943326

A Conformal Circularly Polarized Series-Fed Microstrip Antenna Array Design

Stanislav Ogurtsov and Slawomir Koziel, *Senior Member*, *IEEE*

***Abstract*—A conformal circularly polarized series-fed microstrip array design for broadside radiation is presented. The array aperture under design is conformal to a cylindrical surface of a given radius. The approach we present primarily addresses focusing of the circularly polarized major lobe of the conformal array by proper dimensioning of the aperture spacings. The proposed analytical models yield the values of the element spacings within the series-fed conformal array aperture, and element-specific spacings of the patch radiators within each circularly polarized element. These spacings are critical to produce a broadside circularly polarized major lobe at the design frequency. Subsequently, each array element is equipped with an in-line matching quarter wave transformer. Measured characteristics of the X-band conformal array validate the proposed design approach.**

***Index Terms*—conformal antenna, broadside array, series feed, comb-line antenna, circularly polarized antenna, axial ratio, microstrip array antenna.**

I. Introduction

SERIES-FED comb-line microstrip antenna arrays offer relatively simple layouts featuring compact feeds as well as ease of manufacturing for microwave and millimeter-wave applications. Detailed design studies [1], [2] on comb-line microstrip linear arrays have been conducted with one-wavelength- and half-wavelength-spaced open-end microstrip stub radiators (referred to as co-phase linear apertures), with the quarter-wavelength-spaced series-fed radiators (referred to as quadrature-phase linear apertures), as well as with their combination in the corporate feed of a linearly polarized planar aperture. In these studies, the microstrip feeds terminated on the matching load (the case of travelling wave operation) and with the open-end feeds (the case of resonant operation) had been considered for design of apertures with non-uniform amplitude excitations for reduced sidelobes [1], [2]. The leaky-wave concepts have been applied to the analysis and design of comb-line antennas [3]-[6] as well. The issue of increased reflection loss of comb-line arrays with co-phase excitation has been addressed using quarter-wavelength transformers [5], reflection-cancelling slits [7], stubs [8], and stubbed elements [9, 10]. The stubbed elements were also used to control coupled power and thus to reduce the sidelobe levels [9], [10]. Furthermore, microstrip comb-lines have been considered for circularly polarized broadside operation of linear arrays [11], [12]. Series-fed composite right/left-handed transmission line leaky-wave microstrip antennas were reported for conformal applications [13], [14], where dispersion engineering of metamaterial-based sections compensated for the effect of bending on the radiation characteristics.

Contemporary approaches to pattern and polarization control in conformal antenna arrays rely on phase shifters providing a necessary phase weight for the radiation element with a predefined position, in particular, for forming the major lobe and pointing it to a required direction [15]-[20]. Our work contributes to the development of conformal microstrip arrays with circularly polarized broadside sum patterns by dimensioning spacings of the series-fed array aperture. Our approach does not lead to any complications of the antenna layout, i.e., no fine elements, which might be sensitive to manufacturing tolerances, vias, electronically controlled diodes or switches are introduced in the array aperture. Such an approach can be useful for conformal antennas operating in mm-wave frequencies and/or for conformal antennas featuring small aperture footprints, e.g., implemented on high-permittivity microstrip substrates.

To demonstrate our approach in detail, we design an X-band microstrip array which is conformal to a cylindrical surface of a particular radius. The tasks of co-phase excitation for the broadside and circularly polarized major lobe radiation are addressed with the proposed analytical models. By solving the model equations, one obtains spacing of the array elements within the array aperture and the element-specific spacings of the patch radiators within each element. Full-wave electromagnetic (EM) simulations are included in the described approach.

The novelty and the technical contribution of this work include: (i) focusing of the major lobe of the conformal series-fed array by dimensioning the aperture spacings; (ii) ensuring circular polarization of the focused major lobe of the conformal series-fed array by dimensioning the element-specific spacings of the two radiators within each circularly polarized element; (iii) development of analytical equations to calculate all dimensions necessary for the tasks of focusing and ensuring circular polarization for an array conformal to a cylindrical

Manuscript received April 17, 2019. This work was supported in part by the Icelandic Centre for Research (RANNIS) Grant 174114051, and by the National Science Centre of Poland Grant 2017/27/B/ST7/00563.

S. Ogurtsov and S. Koziel are with School of Science and Engineering, Reykjavik University, Menntavegur 1, 101 Reykjavik, Iceland. (e-mail: koziel@ru.is). S. Koziel is also with the Faculty of Electronics, Telecommunications, and Informatics, Gdansk University of Technology, Gdansk, Poland.

This article has been accepted for publication in a future issue of this journal, but has not been fully edited. Content may change prior to final publication. Citation information: DOI 10.1109/TAP.2019.2943326, IEEE Transactions on Antennas and Propagation

surface of a given radius; (iv) utilizing the analytical model equations within a systematic design process.

For the sake of validation, the reflection and radiation responses of the manufactured prototype of the designed conformal antenna array have been measured in an antenna anechoic chamber.

II. Antenna Configuration

Consider a microstrip antenna array consisting of ten series-fed elements in a flat formation [12], as shown in Fig. 1(a). Each element has two radiators [12] as shown in Fig 2. The radiators should be fed in quadrature at the design frequency, so that each element produces circular polarization. Feeding in a quadrature can be achieved for the flat formation if the radiators are one-quarter guided wavelength apart center to center at the design frequency [12]. Similarly, feeding the elements in phase for the broadside radiation can be achieved for the flat formation if the elements are distributed a wavelength apart (center to center). However, if the microstrip antenna array shown in Fig. 1(a) is adapted to conform a cylindrical surface, as shown in Fig 1(b), pointing the major lobe in a certain direction, broadside at the design frequency in this work, as well as forming the major lobe results in the phase taper which is specific to the array aperture and the direction of the major lobe [15]. In general, such phase tapers are realized using phase-shifting networks [15]-[20].

In the considered case of Fig. 1(b), i.e., for series-fed conformal apertures energized through the same transmission line, the requirement of pointing the major lobe broadside results in particular element spacings being different from one wavelength. Similarly, the conformal geometry of the aperture requires the spacing of radiators within the circularly polarized element to differ from one-quarter guided wavelength. A detailed formulation and means of calculating the elements' spacings within the aperture as well as the radiators' spacings within each element (cell) are described in the next section.

III. Design Process and Models

In this work, it is assumed that the progressive phase shift between the adjacent circularly polarized (CP) elements should be -2π radians towards the broadside direction. For example, in the flat formation, the elements should be spaced one guided wavelength at the design frequency, λ_g. Extensions for integer numbers of -2π radians will be specified and justified for the conformal formations as well. The patch radiators of the element should be $-\pi/2$ radians out of phase for CP broadside radiation, e.g., one-quarter guided wavelength at the design frequency, $\lambda_g/4$, for the flat formation. Further, all elements are fed with a 50 ohm microstrip line and defined here with the same values of radiators' dimensions, v_r, w_r, and u_r. The broadside direction for the conformal formation shown in Fig 1(b) is defined as the direction out of the page.

The design process can be outlined in major steps as follows:

i. For a particular microstrip substrate, obtain the propagation constant β_g of the microstrip at the design frequency using a transmission line (TL) calculator or a full-wave EM simulation, e.g., using those of CST MWS [21]. Calculate the corresponding guided wavelength λ_g and the effective permittivity ε_g;
ii. For a given radius r_c of the cylindrical surface the array should conform to, and for the progressive phase shift between the adjacent CP elements towards the broadside direction of -2π radians, calculate all element spacings s_n by solving equations of the analytical model;
iii. For a given radius of the cylindrical surface and the $-\pi/2$ radians phase shift (toward the broadside direction) between the radiators of the CP elements, calculate all radiators' spacings l_{rn} by solving corresponding equations of the analytical model, e.g., using Matlab [22];
iv. Determine dimensions of the radiators, v_r, w_r, and u_r, resulting in acceptable broadside radiation and reflection responses of the element without a transformer. For that purpose, one can use EM simulations of the element with radiators spaced $\lambda_g/4$;
v. Determine dimensions s_{tn}, l_{tn}, and w_{tn}, of the transformers, to minimize reflection from every element having a specific radiator spacing l_{rn} (calculated at Step iii);
vi. Define and simulate the EM model of the conformal array with the aperture and element dimensions determined at the previous steps using a full-wave modeler/solver, e.g., CST MWS [21].

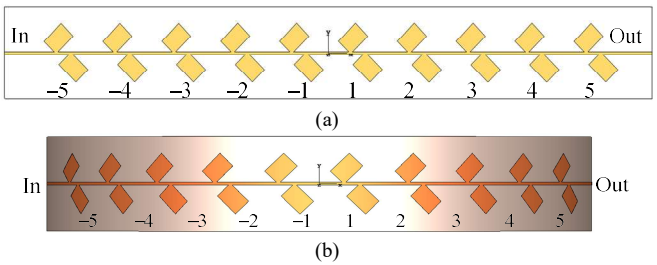

Fig. 1. Left-hand circularly polarized (LHCP) series-fed microstrip antenna array configuration front views: (a) flat formation [12]; (b) conformal formation, considered in this work. Quarter-wave transformers are not shown.

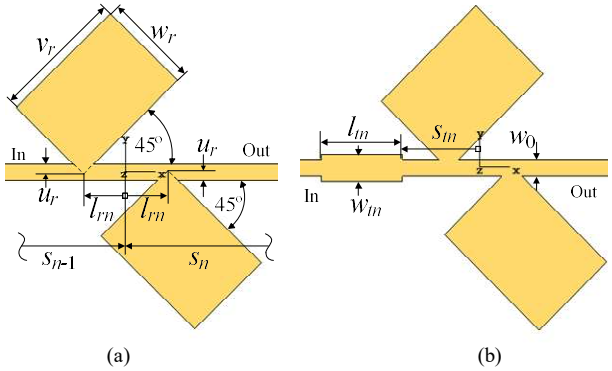

Fig. 2. LHCP array element: (a) radiators' dimensions [12]; (b) quarter-wave transformer's dimensions. Up-stepping (toward the input) transformers ($w_{tn} > w_0$) or down-stepping transformers ($w_{tn} < w_0$) are used depending on an element. Subscript n denotes element-specific dimensions adjusted in this work. s_n stands for the center-to-center spacing between the n-th and (n+1)-th elements as shown in panel (a). The centers are denoted as origins of the XYZ-coordinate system.

This article has been accepted for publication in a future issue of this journal, but has not been fully edited. Content may change prior to final publication. Citation information: DOI 10.1109/TAP.2019.2943326, IEEE Transactions on Antennas and Propagation

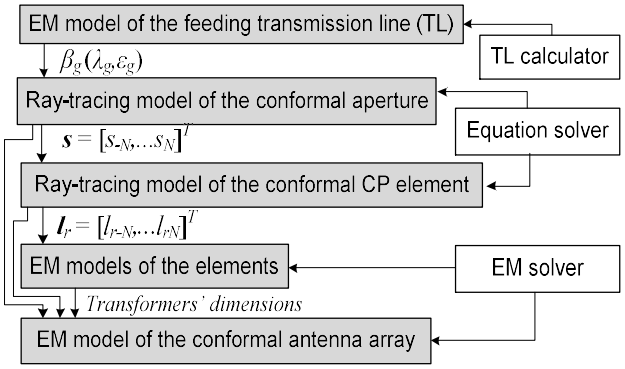

Fig. 3. Conformal CP series-fed microstrip array design flow for focusing the major lobe and ensuring its circular polarization.

The diagram in Fig. 3 lists the utilized models, their evaluation means, and depicts the flow of data. Analytical ray-tracing models described in the next subsections assume omnidirectional elements/radiators.

A. Ray-Tracing Model of the Conformal Aperture

Figure 4 helps to explain the setup of the conformal aperture model which is used at Step ii of the design process. The elements are excited sequentially in the clockwise direction as depicted. The element spacings s_n are all arcs with the curvature radius r_c, and they can be understood (for later implementation) as the lengths of the signal trace metallization between the elements. Spacing s_1 is set to the calculated (or pre-simulated) value of the guided wavelength λ_g at the design frequency.

Requiring a constructive summation towards the zenith from the elements n and $n-1$ and with respect to the excitation order (here, clockwise), e.g., with -2π phase shift toward the zenith, equations for other s_n follow from

$$\beta_g s_n - \beta_0 \Delta_n = 2\pi \tag{1}$$

for the left elements ($n = -2, -3\ldots$) and with

$$\beta_g s_n + \beta_0 \Delta_n = 2\pi \tag{2}$$

for the right elements ($n = 2, 3, \ldots$). In (1) and (2), β_0 stands for the free-space propagation constant at the design frequency. Requirements (1) and (2) can be rewritten as equations for s_n

$$s_n = \lambda_g \pm \frac{r_c}{\sqrt{\varepsilon_g}} \left(\begin{array}{l} \cos\left(\frac{\alpha_1}{2} + \alpha_2 + \ldots + \alpha_{n-1}\right) - \\ \cos\left(\frac{\alpha_1}{2} + \alpha_2 + \ldots + \alpha_{n-1} + \frac{s_n}{r_c}\right) \end{array} \right), \tag{3}$$

where the plus sign in the right-hand-side of (3) should be used for the left elements and the minus sign for the right elements, respectively, whereas $\alpha_k = s_k/r_c$ ($k = 1, -2, \ldots, -(n-1)$ or $k = 1, 2, \ldots, n-1$, respectively). Thus, sequentially solving (3) by starting from element -2 for the left part of the aperture and element 2 for the right part, all conformal spacings become available. The cases of odd number of elements are included in (3) with $\alpha_1 = 0$.

According to (3), the spacings s_n of the left part of the aperture in Fig. 4 are progressively enlarged towards the input while the spacings of the right part are progressively shortened towards the output, all in comparison to the spacings of the flat formation $s_1 = \lambda_g$. Thus, larger spacings resulting in $-2\pi k$ phase shift might be necessary for the right part of the aperture of Fig. 4. In this case the entry λ_g in (3) should be replaced by $k\lambda_g$.

It is worth to note that focusing considerations and, thus, equation (3), also apply for the center-fed travelling-wave arrays, e.g., as those considered in [23] and [24], which could be adopted for conformal applications. For such arrays, the input would be on the z-axis whereas the outputs (matched terminations) would be at the left- and right-most ends of the arc in Fig. 4. In this case, equation (3) should be applied with the – sign for all elements.

B. Ray-Tracing Model of the Conformal Circularly-Polarized Element

Consider the elements consisting of two radiators each as depicted in Fig. 5 for the left and right parts of the array aperture. Requiring a constructive summation towards the zenith for circularly polarized radiation from the radiators of elements n with respect to the excitation order (here, clockwise), i.e., with $-\pi/2$ phase shift towards the zenith, equations for spacings of the radiators follow from

$$\beta_g(l_{rn-} + l_{rn+}) - \beta_0(\Delta_{n-} + \Delta_{n+}) = \frac{\pi}{2} \tag{4}$$

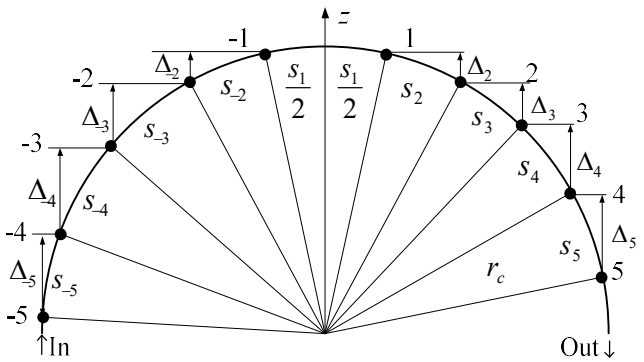

Fig. 4. Conformal array aperture (shown with ten elements as in Fig 1(b)) focused broadside (toward the z-axis). ● denote centers of elements. In this work, centers of elements -1 and 1 are symmetrical with respect to the z-axis.

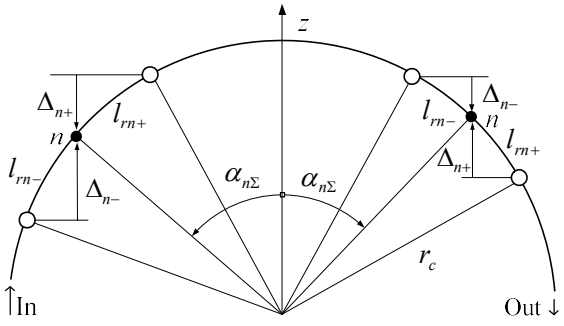

Fig. 5. Conformal array elements focused for CP radiation toward the z-axis. ○ denote radiators. ● denote centers of the elements as in Fig. 4.

This article has been accepted for publication in a future issue of this journal, but has not been fully edited. Content may change prior to final publication. Citation information: DOI 10.1109/TAP.2019.2943326, IEEE Transactions on Antennas and Propagation

for all left elements ($n = -1, -2, \ldots$) and with

$$\beta_g (l_{rn-} + l_{rn+}) + \beta_0 (\Delta_{n-} + \Delta_{n+}) = \frac{\pi}{2} \tag{5}$$

for all right elements ($n = 1, 2, \ldots$). Noticing that (4) and (5) can be satisfied with equal radiator spacing $l_{rn-} = l_{rn+}$ and denoting the spacings with l_{rn}, one obtains from (4) and (5) that

$$l_{rn} = \frac{\lambda_g}{8} \pm \frac{r_c}{\sqrt{\varepsilon_g}} \sin(\alpha_{n\Sigma}) \sin\left(\frac{l_{rn}}{r_c}\right), \tag{6}$$

where + in the right-hand-side of (6) should be used for all left (relative to the zenith) elements and – for all right elements, and $\alpha_{n\Sigma}$ stands for the zenith angle of the element n's center which is already calculated using (3) and depicted in Fig. 5.

It is worth to mention that (6) equally applies to both circular polarization senses, left-hand and right-hand, which are determined by which radiator, upper or lower in Fig. 1(b) and Fig. 2, leads.

More accurate versions of requirements (1) and (2) as well as (4) and (5), and, consequently, equations (3) and (6), can be formulated by accounting for angular dependence complex-valued far-field factors of the elements and radiators, (2.11) or (2.14) of [15]. Such far-field factors are evaluated accurately using full-wave EM simulations, results of which should be coupled with the ray-tracing formulation in this case. Design improvements due to such simulation-enhanced modelling in the presence of other factors, e.g., through-field coupling of radiators, disturbance of microstrip line transmission characteristics due to contacts with patch radiators, etc., will be a subject of our extension work and, therefore, left out of this paper's scope.

IV. Design Example

We design an X-band antenna array comprising ten LHCP elements which are shown in Fig. 2 to demonstrate the design process flow and the operation of the analytical models of Section III in more detail. For that purpose, we adopt 0.635-mm-thick RO3010 microstrip substrate with 17.5μm copper metallization [25].

The RO3010 is a high dielectric constant material; it allows obtaining antenna layouts of reduced dimensions. On the other hand, the following facts regarding the RO3010 permittivity values used in the design process, namely, supplied to the TL calculators and/or EM simulators (e.g., in this work at steps i and iv-vi of the design process outlined in Section III) should be taken into considerations: the apparent ε_r (an isotropic dielectric constant value apparent for a particular test method) depends on an EM field distribution excited in the substrate, substrate thickness, and can varies from lot to lot within a certain range [25]-[27]; in addition, the RO3010 dielectric constant has been experimentally found to be noticeably anisotropic [26], [27].

Contemporary limitations of the EM software utilized for the purpose of this work should be also taken into consideration. These include the lack of possibility to obtain the propagation constants β_g as well as the scalar-valued effective permittivity ε_g of the transmission lines built on anisotropic substrates from either waveguide port simulations or TL calculators, and the lack of possibility to reliably model and simulate bended antenna apertures residing on anisotropic substrates.

Being acknowledged of the above listed facts and typically used values of ε_r we stayed with practical EM modelling means and conducted the design process using the scalar-valued RO3010 dielectric constant ε_r = 10.2 [25], [26] at 10 GHz. The primary design task included pointing the LHCP major lobe boresight; the auxiliary task was to match the antenna array elements for the travelling-wave operation. The conformal antenna with in-line quarter-wave transformers is shown in Fig. 6.

The propagation constant β_g of the 50 ohm feeding microstrip at 10 GHz was evaluated as 558.5 m^{-1} using CST MWS [21]. The center spacing of the array aperture s_1 was set to the guided wavelength λ_g =11.25 mm.

Using the effective permittivity ε_g = 7.0 the element spacings were calculated with eq. (3) as $\boldsymbol{s}$ = [16.89 15.29 13.69 12.33 11.25 10.41 9.76 9.27 8.88]^T mm. Subsequently, the radiator spacings were calculated with (6) as $\boldsymbol{l}_r$ = [2.19 2.02 1.81 1.62 1.47 1.35 1.26 1.16 1.13 1.09]^T mm.

Patches of the element shown in Fig. 2(a) and having the 50 ohm microstrip trace width w_0 = 0.56 mm and the $l_{rn} = \lambda_g/8$ (1.406 mm) was dimensioned for 10 GHz operation with respect to its reflection coefficient and CP radiation characteristics. For this purpose, the element was simulated in the flat formation using the frequency-domain tetrahedral solver of CST MWS [21]. Dimensions of the radiator patches v_r, w_r, and u_r (shown in Fig. 2(a)) providing acceptable characteristics of interest were obtained as 3.3, 4.63, and 0.35, all in mm.

Although the reflection coefficient S_{11} of this element (with the $\lambda_g/4$ mm separation of radiators) was simulated as under –27 dB at 10 GHz and under –10 dB within the frequency range of 9.8 GHz to 10.2 GHz, for the elements with l_{rn} deviated from $\lambda_g/8$ ($\boldsymbol{l}_r$ entries listed in the end of the previous paragraph) the reflection coefficients degrade to –10 dB for the outermost elements in the antenna array aperture. Therefore, quarter-wave transformer sections were added to each element as shown in Fig. 2(b)). The transformer dimensions and positions were obtained as $\boldsymbol{w}_t$ = [0.28 0.29 0.37 0.50 0.56 0.64 0.73 0.85 0.86 0.90]^T mm, $\boldsymbol{l}_t$ = [2.94 2.94 2.91 2.89 *NA* 2.84 2.84 2.82 2.80 2.280]^T mm, and $\boldsymbol{s}_t$ = [2.75 2.62 2.83 3.02 *NA* 2.35 2.61 2.62 2.70 2.69]^T mm using standard microwave circuit means where entries *NA* denote that there is no transformer at the input of the fifth element.

A conformal array was defined as shown in Fig. 6 and simulated for its S-parameters and radiation characteristics using CST MWS [21]. The simulated project was energized and terminated with the microstrip waveguide ports.

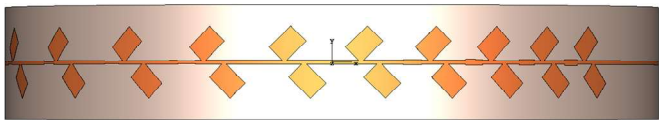

Fig. 6. Designed travelling-wave X-band conformal array on an 8.7 mm by 156 mm RO3010 (0.635 mm). Bending radius is 50 mm. Input on the left.

This article has been accepted for publication in a future issue of this journal, but has not been fully edited. Content may change prior to final publication. Citation information: DOI 10.1109/TAP.2019.2943326, IEEE Transactions on Antennas and Propagation

The selected simulated characteristics of the conformal array are shown in Figures 7 through 11. In particular, Fig. 7(a) shows the effect of dimensioning the conformal array for beam focusing using (3) and for ensuring circular polarization of the major lobe using (6) while Figs. 7(b) and (c) are shown for comparison where Fig. 7(b) corresponds to the flat array shown in Fig. 1(a) with one-wavelength spaced elements, quarter-wavelength spaced radiators, and other parameters as the designed. In contrast to the focused CP pattern of Fig. 7(a), Fig. 7(c) shows the unfocused pattern of the bended array with spacing of elements and radiators as in the flat array.

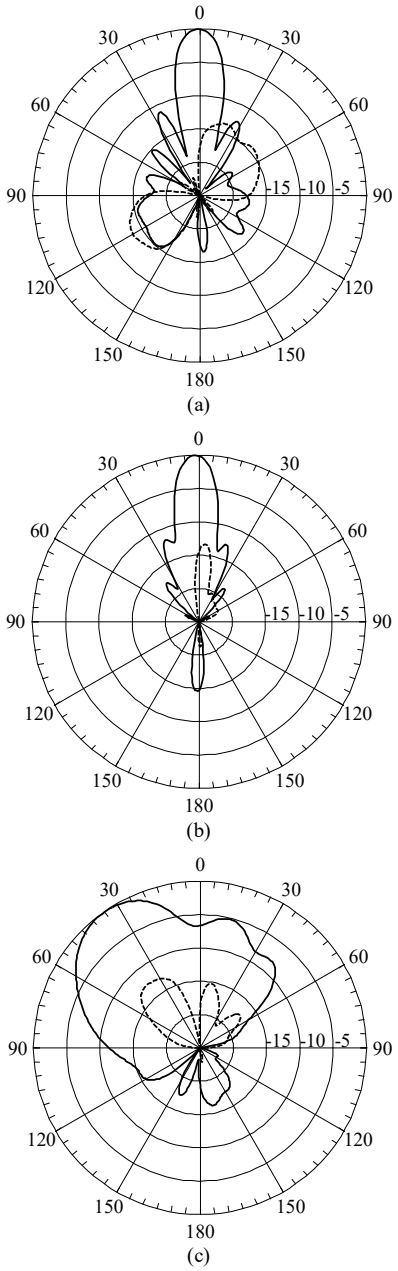

Fig. 7. Simulated patterns at 10 GHz of the LH (—) (primary) and RH (---) circular polarizations: (a) designed conformal array of Fig. 6, 12.3 dBi peak directivity; (b) flat array as of Fig. 1(a) and (c) conformal array as of Fig. 1(b), both with one-wavelength spaced elements, quarter-wavelength spaced radiators, and other parameters as the designed.

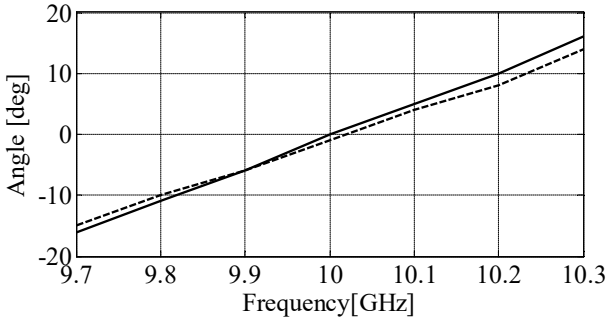

Fig. 8. Simulated direction of the major lobe: designed conformal array (—) and array in the flat formation as of Fig. 1(a) with one-wavelength spaced elements, quarter-wavelength spaced patch radiators, and the other parameters as the designed (---).

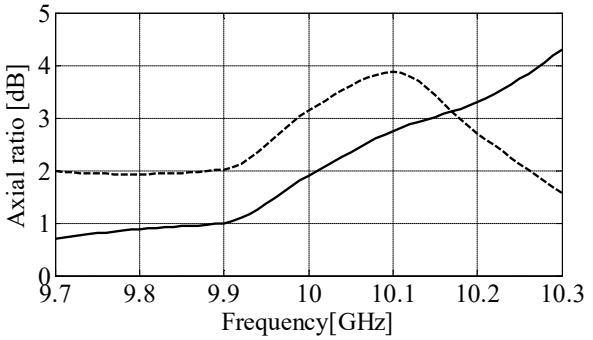

Fig. 9. Simulated axial ratio in the direction of the major lobe maximum: designed conformal array (—) and array in the flat formation as of Fig. 1(a) with one-wavelength spaced elements, quarter-wavelength spaced patch radiators, and the other parameters as the designed (---).

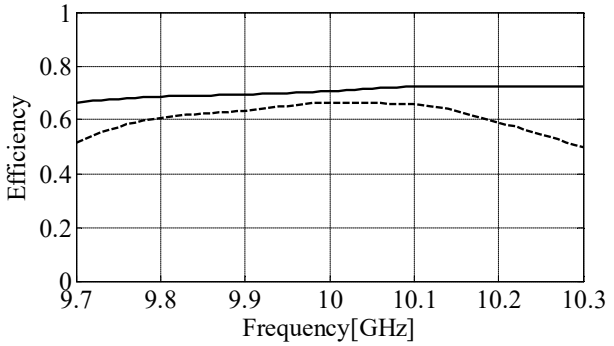

Fig. 10. Simulated radiation (—) and total (---) efficiencies of the designed conformal array.

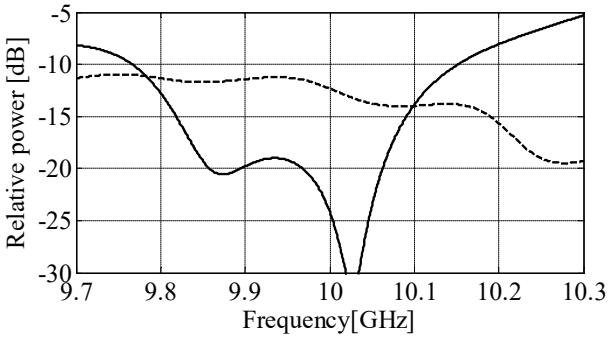

Fig. 11. Simulated reflection (—) and transmission (---) coefficients of the conformal array designed with ε_r = 10.2 [25] of the microstrip substrate.

This article has been accepted for publication in a future issue of this journal, but has not been fully edited. Content may change prior to final publication. Citation information: DOI 10.1109/TAP.2019.2943326, IEEE Transactions on Antennas and Propagation

Figure 8 shows the dependence of the major lobe direction on frequency for the designed conformal array where the conformal array shows almost identical beam scanning behavior in frequency as the flat array which features one-wavelength spaced elements, quarter-wavelength spaced radiators, and other parameters as the designed ones. Figure 9 illustrates that the axial ratio of the designed conformal array in the direction of its major lobe maximum has been enhanced using the model described in Section III.*B*, in particular, it is 1 dB better than that of the corresponding flat array at the design frequency.

The simulated efficiencies of the designed array, shown in Figs. 10 are typical for travelling wave arrays operating over similar frequencies and comprising the comparable number of patch radiators, e.g., [4] and [12], as well as for microstrip antennas residing on high permittivity substrates [12] and [28]. The simulated bandwidth shown in Fig. 11 is about 4 percent and it is mostly determined by those of the microstrip patch radiators [28].

V. Experimental Verification of the Design Approach

A prototype of the designed antenna is shown in Fig. 12. The 0.635 mm thick RO3010 microstrip substrate is 8.7 mm by 156 mm in lateral extends. The antenna arc length is 156 mm from the flange of the input edge-mount 50 ohms SMA connector to the flange of the terminating 50 ohms SMA connector. The length of the antenna aperture from the first to the last patch radiator is 111 mm. The bending radius by upper metallization of the antenna is 50 mm. The prototype was mounted on the acrylic glass fixture and energized through the semi-rigid coaxial cable as shown in Fig. 12. The effect of the semi-rigid cable had been removed with calibration. The prototype had been measured in the Anechoic Chamber of Reykjavik University.

The EM model of the antenna had been upgraded with the SMA connectors and the test fixture. Subsequently, the upgraded EM model had been simulated with various values of ε_r of microstrip substrate. It was determined that ε_r = 10.8 provided the closest approximation of the measured reflection coefficient and radiation patterns as shown in Fig. 13—17.

VI. Discussion

The measured radiation patterns, in particular, major lobe direction, beamwidth, and shape, and the ones simulated with ε_r = 10.8 agree very well as shown in Fig. 14—16, and all together validate the approach to focusing of travelling-wave conformal arrays using the model described in Section III.*A*.

Fig. 12. Measured X-band antenna array on a test fixture: a photograph.

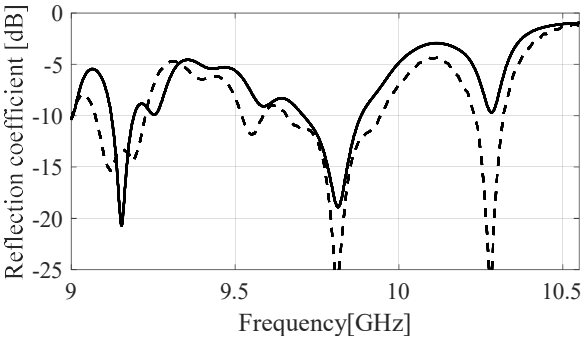

Fig. 13. Reflection coefficient: measured (- - -) and simulated with ε_r = 10.8 of the microstrip substrate (—).

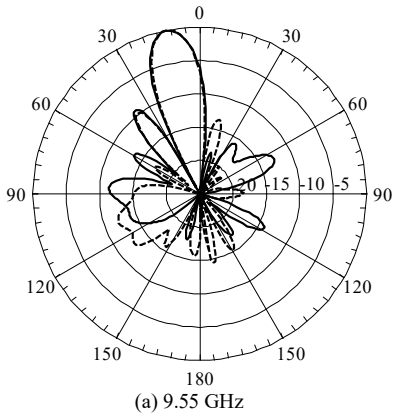

(a) 9.55 GHz

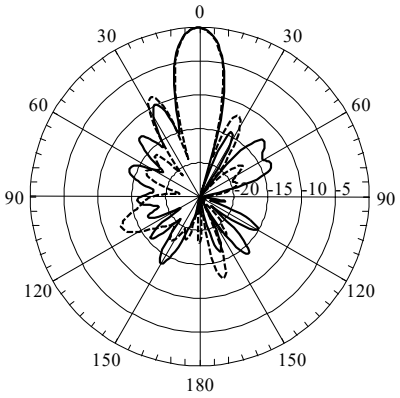

(b) 9.75 GHz

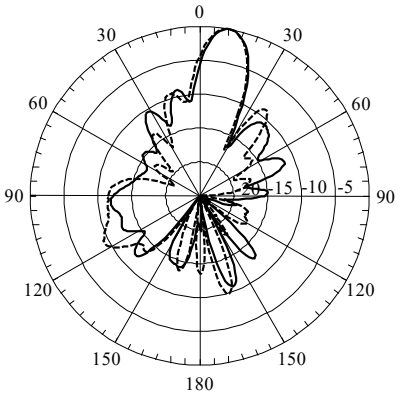

(c) 9.95 GHz

Fig. 14. Normalized LHCP patterns: measured (- - -) and simulated with ε_r = 10.8 of the microstrip substrate (—).

This article has been accepted for publication in a future issue of this journal, but has not been fully edited. Content may change prior to final publication. Citation information: DOI 10.1109/TAP.2019.2943326, IEEE Transactions on Antennas and Propagation

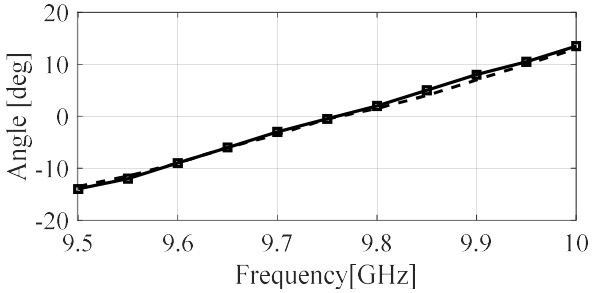

Fig. 15. Direction of the major lobe maximum: measured (- - -) and simulated with ε_r = 10.8 of the microstrip substrate (□—).

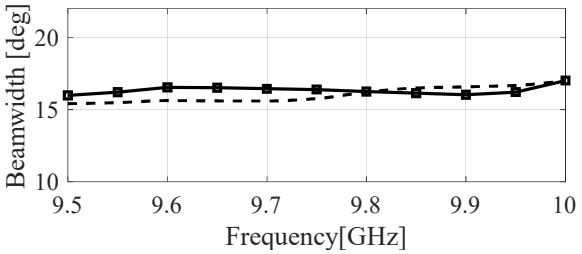

Fig. 16. Major lobe half-power beamwidth: measured (- - -) and simulated with ε_r = 10.8 of the microstrip substrate (□—).

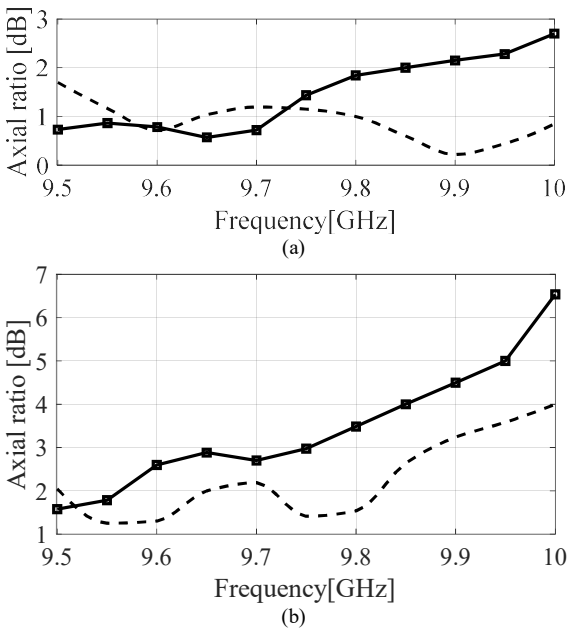

Fig. 17. Axial ratio, measured (- - -) and simulated (□—): (a) toward the major lobe maximum; (b) maximal value over the half-power beamwidth. The simulated characteristics are for ε_r = 10.8 of the microstrip substrate.

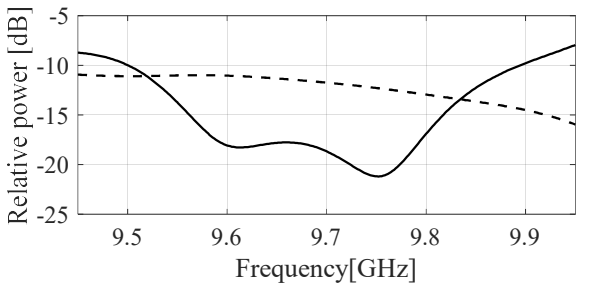

Fig. 18. Simulated reflection (—) and transmission (- - -) coefficients of the conformal array without connectors and with ε_r = 10.8 of the substrate.

The measured axial ratio (AR) at the peak of the major lobe is better than 1.5 dB from 9.55 GHz to 10.00 GHz as shown in Fig. 17(a), and the highest AR over the major lobe half-power beamwidth is under 4 dB from 9.5 GHz to 10.0 GHz and it is 1.5 dB at 9.75 GHz as shown in Fig. 17(b). Thus, both measured AR characteristics validate the model described in Section III.*B* for ensuring the polarization quality of travelling-wave conformal arrays.

The presented conformal design is compared with similar CP microstrip antenna arrays with flat radiation apertures in Table I where one see that the presented design has similar characteristics in overall while being the most compact.

At the same time, comparing the reflection coefficient plots of Fig. 13 and Fig. 18 one can observe the destructive effects the connector-to-microstrip junctions while the scattering parameters simulated with apparent dielectric constant of ε_r = 10.8, shown in Fig. 18, are consistent with those simulated for apparent dielectric constant of ε_r = 10.2 [25], shown in Fig. 11 up to the 0.25 GHz frequency shift. Due to this difference of the nominal dielectric constant of ε_r = 10.2 [25] and the inferred ε_r = 10.8, the radiation characteristics of Figs. 14(a) and 15 are shifted by the same amount of 0.25 GHz in comparison to those of Figs. 7(a) and 8. Also, the total gain was measured as 10.0 dB at 9.75 GHz, and it is consistent to the total gain of 10.5 dB at 10 GHz simulated at the design stage, Section IV, with respect to the frequency shift.

Finalizing our discussion we would like to notice that for design of high-performance conformal series-fed arrays, e.g. ones with low sidelobes, improved efficiencies, broadband impedance bandwidths, etc., i.e., in situations where through-field and through-feed coupling can seriously affect antenna figures of interest, simulation-based tuning and even multi-objective optimization, e.g., as in [32] and [33], will be required to obtain proper amplitude tapers (e.g., using design guidelines of [1]) with respect to several antenna figures of interest. In such cases, the presented models can provide an initial design to be further tuned through numerical optimization. In the same time we want to notice that in this work coupling had been addressed to certain extent by dimensioning of patch radiators in the CP array element prior bending as well as by design and tuning of the impedance transformers which were added in the conformal feed to alleviate the issue of increased reflection from the conformal CP elements with separations of patch radiators deviated from a quarter wavelength (according to Eq. (6)).

It is worth to emphasize that the presented models and approaches, already developed for flat series-fed arrays, namely, for excitation taper design and impedance bandwidth extension, e.g., [1], [8]-[10], can augment each other well for high-performance conformal series-fed array design due to the fact that the former help to adjust radiator spacing in the conformal array aperture while the latter mostly adjust dimensions of the array elements including their feeding elements.

This article has been accepted for publication in a future issue of this journal, but has not been fully edited. Content may change prior to final publication. Citation information: DOI 10.1109/TAP.2019.2943326, IEEE Transactions on Antennas and Propagation

TABLE I
COMPARISON OF THE CONFORMAL CP ARRAY OF THIS WORK WITH SIMILAR FLAT CP MICROSTRIP ANTENNA ARRAYS

Array	Elements	Feed	Footprint [mm × mm]	f_0 [GHz]	Boresight Gain [dB]	3-dB AR BW[b] [%]	10-dB Impedance BW[b] [%]
This work	1×10 dual patches	Travelling-wave microstrip	156 × 9	9.75	10.0	4.0[a]	3(4 no SMA conn.)
[12]	1×12 dual patches	Travelling-wave microstrip	224 × 38	8.72	~12	13	5
[29]	8 concentric patches	Travelling-wave microstrip	100 × 90	10.0	12.5	6.6	~20
[30]	1×10 dual patches	Standing-wave slotted waveguide	188 × 45	10.5	15.9	3.2	4.0
[31]	1×10 dual loops	Standing-wave slotted SIW	168 × 23	10.0	~15	2.8	3.5

[a] the BW value based on the maximum AR over the half-power beamwidth. Boresight AR < 1.5 dB over the impedance BW.
[b] Bandwidth.

VII. CONCLUSION

The paper addressed the problem of design of conformal series-fed microstrip arrays for broadside CP radiation. The presented approach to beamforming and ensuring circular polarization of the major lobe has been experimentally validated. It can be applied to the design of series-fed comb-line linearly and CP arrays conformal to cylindrical surfaces, for pointing the major lobe broadside, as well as to the design of conformal frequency scanning arrays to avoid degradation of the major lobe characteristics without introducing extra circuitry. The proposed models allow completion of the aforementioned tasks using contemporary means of antenna engineering and EM model evaluation.

ACKNOWLEDGMENT

The authors would like to thank Dassault Systèmes, France, for making CST Microwave Studio available for their research. Furthermore, we would like to thank Dr. James C. Rautio of Sonnet Software Ltd. for sharing valuable information about measured permittivity of microstrip substrates.

REFERENCES

[1] J. R. James and P. S. Hall, "Microstrip antennas and arrays. Part 2: New array-design technique," *IEE J. Microwaves, Optics and Acoustics*, vol. 1, no. 5, pp. 175-181, Sep. 1977.

[2] J. R. James and G. J. Wilson, "Microstrip antennas and arrays. Part 1: Fundamental action and limitations," *IEE J. Microwaves, Optics and Acoustics*, vol. 1, no. 5, pp. 165-174, Sep. 1977.

[3] S. Paulotto, P. Baccarelli, F. Frezza and D. R. Jackson, "A Novel technique for open-stopband suppression in 1-D periodic printed leaky-wave antennas," *IEEE Trans. Antennas Propag.*, vol. 57, no. 7, pp. 1894-1906, July 2009.

[4] J. T. Williams, P. Baccarelli, S. Paulotto and D. R. Jackson, "1-D combline leaky-wave antenna with the open-stopband suppressed: design considerations and comparisons with measurements," *IEEE Trans. Antennas Propag.*, vol. 61, no. 9, pp. 4484-4492, Sept. 2013.

[5] S. Otto and C. Caloz, "Solving the broadside radiation issue in periodic leaky-wave antennas," in *Proc. 2015 IEEE 4th Asia-Pacific Conf. Antennas Propag. (APCAP)*, Kuta, Indonesia, 2015, pp. 629-631.

[6] C. Caloz, D. R. Jackson, and T. Itoh, "Leaky-wave antennas," in *Frontiers in Antennas: Next Generation Design & Engineering*, ch. 9, F.B. Gross, Ed. New York, NY, USA: McGraw-Hill, 2011, pp. 339–379.

[7] Y. Hayashi, K. Sakakibara, M. Nanjo, S. Sugawa, N. Kikuma and H. Hirayama, "Millimeter-wave microstrip comb-line antenna using reflection-canceling slit structure," *IEEE Trans. Antennas Propag.*, vol. 59, no. 2, pp. 398-406, Feb. 2011.

[8] S. T. Choi and Y. H. Kim, "Microstrip travelling wave combline array antenna with reflection compensation," *Electron. Lett.*, vol. 42, no. 21, pp. 1196-1197, 12 Oct. 2006.

[9] S. Afoakwa and Y. Jung, "Wideband microstrip comb-line linear array antenna using stubbed-element technique for high sidelobe suppression," *IEEE Trans. Antennas Propag.*, vol. 65, no. 10, pp. 5190-5199, Oct. 2017.

[10] S. Sugawa, K. Sakakibara, N. Kikuma and H. Hirayama, "Low-sidelobe design of microstrip comb-line antennas using stub-integrated radiating elements in the millimeter-wave band," *IEEE Trans. Antennas Propag.*, vol. 60, no. 10, pp. 4699-4709, Oct. 2012.

[11] K. Hirose, T. Sukegawa, Y. Uchikawa and H. Nakano, "A circularly polarized open loop antenna with application to an array fed by a microstrip comb line," in Proc. *2008 IEEE Antennas Propag. Soc. Int. Symp.*, San Diego, CA, 2008, pp. 1-4.

[12] T.R. Cameron, A.T. Sutinjo and M. Okoniewski, "A circularly polarized broadside radiating "Herringbone" array design with the leaky-wave approach," *IEEE Antennas Wireless Propag. Lett.*, vol. 9, pp. 826-829, 2010.

[13] M.R. Hashemi and T. Itoh, "Dispersion engineered metamaterial-based transmission line for conformal surface application," in *2008 IEEE MTT-S Int. Microw. Symp. Dig.*, Atlanta, GA, USA, 2008, pp. 331-334.

[14] M. R. Hashemi and T. Itoh, "Electronically controlled metamaterial-based leaky-wave transmission-line for conformal surface applications," in *2009 IEEE MTT-S Int. Microw. Symp. Dig.*, Boston, MA, 2009, pp. 69-72.

[15] L. Josefsson and P. Persson, *Conformal Array Antenna Theory and Design,* Hoboken, NJ, USA: John Wiley & Sons, 2006, pp. 20–22.

[16] T. J. Seidel, W. S. T. Rowe and K. Ghorbani, "Passive compensation of beam shift in an array on a bending surface," *2011 8th European Radar Conference*, Manchester, 2011, pp. 85-88.

[17] B. D. Braaten et al., "A self-adapting flexible (SELFLEX) antenna array for changing conformal surface applications," *IEEE Trans. Antennas Propag.,* vol. 61, no. 2, pp. 655-665, Feb. 2013.

[18] B. D. Braaten, S. Roy, I. Irfanullah, S. Nariyal and D. E. Anagnostou, "Phase-compensated conformal antennas for changing spherical surfaces, *IEEE Trans. Antennas Propag.*, vol. 62, no. 4, pp. 1880-1887, April 2014.

[19] B. D. Braaten, S. Roy, Irfanullah, S. Nariyal and D. E. Anagnostou, "An autonomous self-adapting conformal array for cylindrical surfaces with a changing radius," *2014 IEEE Antennas and Propagation Society International Symposium (APSURSI)*, Memphis, TN, 2014, pp. 1784-1785.

[20] H. Xu, J. Cui, J. Duan, B. Zhang and Y. Tian, "Versatile conical conformal array antenna based on implementation of independent and endfire radiation for UAV Applications, " *IEEE Access*, vol. 7, pp. 31207-31217, 2019.

[21] CST Microwave Studio, ver. 2018, Dassault Systèmes, 2018, France.

[22] Matlab R2017a, The MathWorks, Inc., 2017, Natick, MA, USA.

[23] K. Sakakibara, A. Kunita, D. Kawase, N. Kikuma, H. Hirayama and K. Seo, "Broadband millimeter-wave microstrip comb-line antenna using corporate feeding system," in Proc. *2011 41st European Microwave Conference*, Manchester, 2011, pp. 902-905.

[24] Y. Mouri, S. Kitanaka, K. Shida, K. Sakakibara and N. Kikuma, "Traveling-wave design of cross-junction power-dividers for two-dimensional microstrip planar array with 45-degree polarization in

submillimeter-wave band," in Proc. *2016 International Symposium on Antennas and Propagation (ISAP)*, Okinawa, 2016, pp. 756-757.

[25] "RO3000 Series Circuit Materials," Data Sheet. [Online]. Available: https://www.rogerscorp.com/documents/722/acs/RO3000-Laminate-Data-Sheet-RO3003-RO3006-RO3010.pdf, Accessed on: Mar 29, 2019.

[26] "General Information of Dielectric Constant for RT/duroid® 6010.2LM and RO3010™ High Frequency Circuit Materials," [Online]. Available: https://www.rogerscorp.com/documents/2379/acs/General-Information-of-Dielectric-Constant-for-RT-duroid-6010-2LM-RO3010-High-Frequency-Circuit-Materials.pdf, Accessed on: Apr 2, 2019.

[27] J. C. Rautio, "Measurement of uniaxial anisotropy in Rogers RO3010 substrate material," in Proc. *2009 IEEE International Conference on Microwaves, Communications, Antennas and Electronics Systems* (*COMCAS 2009*),Tel Aviv, 2009, pp. 1-4.

[28] D.R. Jackson, "Microstrip antennas," *in Antenna Engineering Handbook*, *4th edition,* ch. 7, J.L. Volakis, Ed. New York, NY, USA: McGraw-Hill, 2007.

[29] C. Min and C.E. Free, "Analysis of traveling-wave-fed patch arrays," *IEEE Trans. Antennas Propag.*, vol. 57, no. 3, pp. 664-670, March 2009.

[30] J. Xu, M. Wang, H. Huang and W. Wu, "Circularly polarized patch array fed by slotted waveguide," *IEEE Antennas Wireless Propag. Lett.*, vol. 14, pp. 8-11, 2015.

[31] L. Lu, Y. Jiao, Z. Weng, H. Zhang and C. Cui, "Design of Low-Sidelobe Circularly Polarized Loop Linear Array Fed by the Slotted SIW," *IEEE Antennas Wireless Propag. Lett.*, vol. 16, pp. 537-540, 2017.

[32] S. Koziel and S. Ogurtsov, *Simulation-Based Optimization of Antenna Arrays*, London, UK: World Scientific Publishing Ltd., 2019, pp. 301-355.

[33] S. Koziel and A. Bekasiewicz, *Multi-Objective Design of Antennas Using Surrogate Models*, London, UK: World Scientific Publishing Ltd., 2017, pp. 156-166.

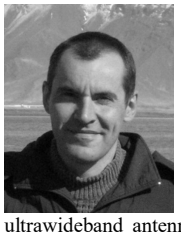

Stanislav Ogurtsov received the degree of physicist from Novosibirsk State University, Novosibirsk, Russia, in 1993, and the Ph.D. degree in electrical engineering from Arizona State University, Tempe, in 2007. He is currently a postdoctoral researcher at the Electromagnetic Optimization and Modeling Center, Reykjavik University, Iceland. His research interests include simulation-driven computer aided design of RF, microwave, and millimeter-wave circuits, ultrawideband antennas, computational electromagnetics, modeling of high-speed digital circuits, and material characterization.

Slawomir Koziel received the M.Sc. and Ph.D. degrees in electronic engineering from Gdansk University of Technology, Poland, in 1995 and 2000, respectively. He also received the M.Sc. degrees in theoretical physics and in mathematics, in 2000 and 2002, respectively, as well as the PhD in mathematics in 2003, from the University of Gdansk, Poland. He is currently a Professor with the School of Science and Engineering, Reykjavik University, Iceland. His research interests include CAD and modeling of microwave and antenna structures, simulation-driven design, surrogate-based optimization, space mapping, circuit theory, analog signal processing, evolutionary computation and numerical analysis.